To what extent do sea-ice algae affect the modelled transmittance of photosynthetically active radiation (PAR) to the ice-ocean interface?

Benjamin H. Redmond Roche and Martin D. King

Centre of Climate, Ocean and Atmosphere, Department of Earth Sciences, Royal Holloway, University of London, Egham, Surrey TW20 0EX, UK

Abstract

Photosynthetically active radiation (PAR) at the ice-ocean interface is critical for primary production. The value of PAR is affected by the thickness of snow and sea ice, with additional absorbers (e.g. algae) further attenuating PAR. Sea-ice algae exhibit a substantial geo-temporal variance in column-integrated concentration (0–500 mg chl-a m^{-2}) and are typically present within the bottom 0.01–0.2 m of sea ice. PAR transmittance is affected by algae concentrations and vertical thicknesses of ice algal layers. Small column-integrated concentrations of chl-a ($\sim$<10 mg chl-a m^{-2}) have a negligible effect on the value of PAR transmittance, and large column-integrated concentrations of chl-a ($\sim$>10 mg chl-a m^{-2}) can significantly reduce the value of PAR transmittance. Large column-integrated concentrations of chl-a need consideration when calculating PAR transmittance in areas of high sea-ice algae biomass (e.g. the 'interior' shelves of the Arctic Ocean, the Canadian Arctic and Antarctica).

1. Introduction

Sea-ice algae generate 10% of total marine-produced carbon and can cause sea ice to host the highest algal cell and chlorophyll concentrations of any marine environment (Tedesco and Vichi, 2014; Arrigo, 2017; Lund-Hansen and others, 2021). The presence of contaminants such as black carbon (e.g. Marks and King, 2013), sediment (e.g. Light and others, 1998; Gradinger and others, 2009), crude oil (e.g. Redmond Roche and King, 2022) or organisms (e.g. Fritsen and others, 1992, 2011) can affect the apparent optical properties of sea ice, including albedo, transmittance, absorption and extinction of light. Photosynthetically active radiation (PAR, wavelength range 400–700 nm) is utilised by autotrophs for photosynthesis and is a critical component of the polar ecosystems, with ice algae being light-limited during the winter and later nutrient-limited once there is sufficient PAR (e.g. Cota and others, 1991; Duarte and others, 2015; Leu and others, 2015; Weckström and others, 2020); other factors such as temperature, salinity and iron can also limit production. PAR at the ice-ocean interface is primarily controlled by snow thickness and, to a lesser extent, by sea-ice thickness (e.g. Mundy and others, 2007). The transmittance of PAR (the fraction of incident light which is transmitted) to the ice-ocean interface can also be considerably affected by the presence of sea-ice algae, with microalgae frequently being the principal absorbing material in sea ice and responsible for up to 25–90% of attenuation between 400 and 550 nm in first-year sea ice (Fritsen and others, 1992, 2011; Light and others, 2015). The presence of ice algae may also affect the physical properties of sea ice and heat the sea ice through increased light absorption (Zeebe and others, 1996). PAR availability at the ice-ocean interface is a fundamental constraint on marine primary production in the water column in the polar regions (Popova, 2010) and potentially even on celestial bodies (e.g. Reynolds and others, 1983; Hand and others, 2009; France and others, 2010). Therefore, parameterising the effect sea-ice algae have on PAR transmittance may be important to understand how sea-ice algae can affect the light availability for primary production beneath the ice (e.g. Petrich and others, 2012; Ehn and Mundy, 2013; Katlein and others, 2014; Hill and others, 2022).

Columnar sea ice has a lamellar crystal structure to which inclusions (e.g. brine pockets, gas bubbles, contaminants) are usually aligned, resulting in sea ice scattering light anisotropically and predominantly downwards (Trodahl and others, 1987; Petrich and others, 2012; Katlein and others, 2014). Previous studies have utilised simple Beer–Lambert exponential decay to predict the propagation of PAR in sea ice and snow (e.g. Grenfell and Maykut, 1977; Tedesco and others, 2014; Stroeve and others, 2021; Lim and others, 2022); however, measurements (e.g. King and others, 2005; Light and others, 2015) have shown that this can provide an inaccurate attenuation profile for non-optically thick sea ice (see Warren, 2019 for a detailed description). Other studies (e.g. King and others, 2005; Redmond Roche and King, 2024) have shown that dark layers in the base of the ice or present below the ice can affect the intensity of PAR throughout sea ice. Concentrations of sea-ice algae exhibit substantial geo-temporal variance, with column-integrated biomass concentrations from the bottom of ice-core sections ranging in chlorophyll a (chl-a, a proxy for ice algae biomass) between

<2 mg chl-a m^{-2} in Greenlandic fjords, 7 mg chl-a m^{-2} in the Central Arctic, 53.8 mg chl-a m^{-2} in the European Arctic and 340 mg chl-a m^{-2} in the Canadian Arctic during maximum bloom conditions (Søgaard and others, 2010, 2019; Leu and others, 2015, and references therein). In the Antarctic, up to 500 mg chl-a m^{-2} has been recorded in sea ice (Riaux-Gobin and others, 2000) and up to 1090 mg chl-a m^{-2} has been recorded in the sub-ice platelet layer (Arrigo, 2017). Sea-ice algae can grow at extremely low light fluxes (0.17 µmol m^{-2} s^{-1}) (Hancke and others, 2018) under thick snow cover and may begin growing as early as February in the Arctic Ocean (Stroeve and others, 2021). Sea-ice algal blooms coincide with increasing PAR (∼5 µmol m^{-2} s^{-1}) between the end of winter and the beginning of sea-ice melt when basal ice layers begin to slough off (Cota and Smith, 1991; Perovich and others, 1993; Hill and others, 2022). Blooms in the Arctic Ocean may also experience bimodal chl-a peaks in March and July (Melnikov and others, 2002). The highest chl-a concentrations are found in the basal layers of sea ice, from the skeletal layer extending vertically up to ∼0.2 m. Typically, ∼95% of algal biomass is located near the ice-ocean interface in the bottom 0.02 m (e.g. Welch and Bergmann, 1989; Perovich and others, 1993; Lavoie and others, 2005); however, different vertical distributions in biomass can occur in the base (0.2 m) and interior of sea ice. The effects of these varying distributions on PAR transmittance are poorly quantified in optical modelling studies (e.g. Lange and others, 2015; Cimoli and others, 2017).

Therefore, while many studies have considered how specific measured concentrations of chl-a affect PAR transmittance (e.g. Arrigo and others, 1991; Perovich and others, 1993, 1998; Mundy and others, 2007), the work presented here aims to use a coupled atmosphere-sea ice/snow radiative-transfer model to parameterise how the variance in column-integrated concentration (0–500 mg chl-a m^{-2}) in measured ice algal biomass can affect PAR transmittance to the ice-ocean interface during winter, spring and summer sea ice and snow conditions. The study also aims to assess how different vertical distributions of sea-ice algae in the base of sea ice (0.01–0.08 m thick layers) and in the middle of sea ice (0.02–0.04 m thick layers) affect PAR transmittance throughout sea ice while keeping the volumetric concentration of algae constant. A visual description of the structure will be shown later in Figure 4.

2. Methods

The radiative-transfer modelling was undertaken using the Tropospheric Ultraviolet-Visible Radiation Model (TUV-snow) (Madronich and Flocke, 1998; Lee-Taylor and Madronich, 2002), an eight-stream DISORT algorithm (Stamnes and others, 1988) that calculates irradiance and photon flux parameters from the top of the atmosphere to the ice-ocean interface, similar to other publically available models (e.g. Flanner and others, 2021). The model is separated into 201 layers, comprising a 62-layer atmosphere (90 km thick), 20-layer snowpack (0.2 m thick) and 119-layer ice pack (2 m thick). The layers are assumed to be horizontally homogeneous with a wavelength-dependent absorption cross section, σ_{abs}, wavelength-independent scattering cross section, σ_{scatt}, asymmetry factor, g, for snow (0.89) and sea ice (0.98) (Mobley and others, 1998), and snow and sea-ice densities, ρ, listed in Table 1. The sea ice and snow matrix control light scattering while the ice, a typical Arctic black carbon mass ratio for snow (10 ng g^{-1}) and sea ice (5.5 ng g^{-1}) (Jiao and others, 2014; Warren, 2019), and the varying concentrations of chl-a control the absorption in the PAR wavelength range. Scattering from black carbon particles and algae is not considered here as they are very minor compared to the scattering from the snow and sea-ice matrix (Perovich, 1996; Mobley and others, 1998). The TUV-snow model calculates the downwelling PAR for all layers in the model, and these are presented in this study as an integrated 'flat plate' PAR equal to an irradiance summed over 400–700 nm. The transmittance of PAR, T, is the value of downwelling PAR at that ice-ocean interface, PAR$_{ice-ocean}$, relative to the value of downwelling PAR at the snow surface, PAR$_{surf}$, (T = PAR$_{ice-ocean}$/PAR$_{surf}$). The TUV-snow model has previously been shown to reproduce light transmittance and reflectance in control laboratory-grown sea ice (e.g. Marks and others, 2017), and all modelling has been kept consistent with previous studies (Redmond Roche and King, 2022, 2024), where a comprehensive description is provided.

The sea ice and snow are separated into three layers: an interior ice layer below freeboard, a drained ice layer above freeboard and a homogeneous overlying snowpack. The freeboard is calculated assuming the sea ice is in hydrostatic equilibrium with a sea-ice density of 920 kg m^{-3}, a snow density of 320 kg m^{-3} and a seawater density of 1027 kg m^{-3}, consistent with previous studies (e.g. Alexandrov and others, 2010; Zhang and others, 2020; Redmond Roche and King, 2024). The sea ice and snow are modelled under three scenarios: winter (≪0°C), spring (<0°C) and summer (≥0°C), consistent with Redmond Roche and King (2024) and comparable with phases 1, 2 and 3 described by Vérin and others (2022). The density of sea ice can vary (700–950 kg m^{-3}) (e.g. Perovich, 1990, 1996); however, here, it is 920 kg m^{-3} for all scenarios to be consistent with the freeboard approximation (Alexandrov and others, 2010; Zhang and others, 2020) and to allow for a direct comparison of the optical effects of the algae in different sea-ice thicknesses. While the value of σ_{scatt} of sea ice can be variable (Grenfell and Maykut, 1977; Perovich, 1990, 1996; King and others, 2005; Light and others, 2008, 2022; Stroeve and others, 2021), the three scenarios have been modelled in accordance with the average vertical scattering profiles presented in Figure 8 of Light and others (2015). Bare sea-ice conditions are also considered in this study, however, melt ponds are not considered (e.g. Light and others, 2008, 2015, 2022; Lamare and others, 2023). The snow density and value of σ_{scatt} differ between the three scenarios, with the winter, spring and summer scenarios being characterised by cold polar/fresh (0.1–0.5 mm grains), coastal windpack/windslab (0.5–2 mm grains) and melting/melt form snow types (2–5 mm grains), respectively (e.g. Grenfell and others, 2002; France and others, 2011; Marks and King, 2014; Lamare and others, 2016; Warren, 2019; Vérin and others, 2022).

The absorption spectrum of sea ice and snow (Warren and Brandt, 2008) is small at shorter wavelengths (∼300–500 nm) and small inclusions of contaminants can considerably modify light absorption (e.g. Warren, 1982; Light and others, 1998; Doherty and others, 2010; Réveillet and others, 2022). Indeed, it

Table 1. Scattering cross-section (σ_{scatt}) and density (ρ) values for all modelled sea ice and snow layers

	Winter scenario		Spring scenario		Summer scenario	
	σ_{scatt}/m^2 kg^{-1}	ρ/kg m^{-3}	σ_{scatt}/m^2 kg^{-1}	ρ/kg m^{-3}	σ_{scatt}/m^2 kg^{-1}	ρ/kg m^{-3}
Snow layer	20	300	7.5	400	1.25	500
Drained layer	0.3	920	0.3	920	0.3	920
Interior layer	0.03	920	0.03	920	0.03	920

Grenfell and Maykut (1977); Perovich (1990, 1996); Grenfell and others (2002); King and others (2005); Light and others (2008, 2015, 2022); France and others (2011); Marks and King (2014); Lamare and others (2016); Warren (2019); Stroeve and others (2021); Vérin and others (2022).

is often necessary to include small concentrations of black carbon, which has a relatively wavelength-independent absorption cross section when using radiative-transfer models to increase attenuation coefficients to match natural measurements of sea ice and snow (e.g. Warren, 1982; Mundy and others, 2007). The absorption spectrum of sea-ice algae is dominated by the pigment chl-a, which has a strong wavelength dependence, with a broad peak typically centred at 440 nm and a narrow peak centred at 680 nm (Arrigo and others, 1991). Figure 1 shows the typical chl-a absorption cross sections for sea-ice algae from both the Arctic and Antarctic (Perovich, 1991; Arrigo and others, 1991; Mundy and others, 2007, 2011; Fritsen and others, 2011; Arrigo, 2017; Wongpan and others, 2018), in addition to phytoplankton chl-a (Bricaud and others, 1995), and phytoplankton photoprotectant and photosynthetic carotenoid pigment (Bidigare and others, 1990). The absorption cross section of sea-ice algae is dependent on the ratio of pigments, which can lead to a packaging effect where the absorption may be flattened (e.g. Morel and Bricaud, 1981; Wang and others, 2020). Sea-ice algae can increase or decrease their photosynthetic efficiency in response to changing PAR availability, which can lead to a packaging effect around 450–550 nm as the ratio of accessory pigments increases (Arrigo and others, 1991); however, chl-a is the dominant pigment present in sea-ice algae (Wang and others, 2020). Consequently, it is complex to accurately quantify the absorption cross section of sea-ice algae (e.g. SooHoo, 1987; Light and others, 2015) as it is dependent on the concentration of pigments, so this study utilises the chl-a cross section presented in Mundy and others (2007) as a representative spectrum and wavelength-integrated PAR transmittance (T) is considered. Therefore, the study presented here will examine (i) the response of T to increasing chl-a column-integrated concentrations (0–500 mg chl-a m^{-2}) in the bottom 0.02 m of sea ice and (ii) the response of T through sea ice under a fixed volumetric chl-a concentration vertically distributed in the basal 0.01, 0.02, 0.04 and 0.08 m of the sea ice, in addition to 0.02 and 0.04 m thick internal layers at 1 m.

3. Results and discussion

3.1. The response PAR transmittance to varying column-integrated concentrations of Chl-a

The transmittance of PAR through a 0.2 m thick snowpack and a 2 m thick sea ice is shown as an exemplar for the summer (a), spring (b) and winter (c) scenarios in Figure 2. The interior layer of the sea ice is 1.85 m thick, and the drained layer is 0.15 m thick, assuming that the sea ice is in hydrostatic equilibrium (Alexandrov and others, 2010; Zhang and others, 2020). When no algae is present, the PAR decreases with depth in the snow and sea-ice layers, with maximum modelled values of 908, 866 and 708 µmol m^2 s^{-1} at the snow surface for the winter, spring and summer scenarios, respectively. The values of PAR decrease to 3, 6 and 26 µmol m^2 s^{-1} at the ice-ocean interface, respectively. Note, that the differences in surface values of PAR between the scenarios are due to the increased value of σ_{scatt} in colder snow packs where the snow grain size is small. The values of T are 0.0033, 0.0069 and 0.037 for the winter, spring and summer scenarios, respectively; as the snow layers are highly scattering relative to the sea ice, they are responsible for 99, 98 and 90% of the attenuation of surface radiation, respectively.

As chl-a concentrations increase in the bottom 0.02 m layer of the sea ice, the attenuation of PAR significantly increases, and the value of T decreases. Figure 2 shows that as basal concentrations of chl-a increase, the transmittance value relative to the algae-free sea ice, T_{Rel}, decreases to between ∼99.4% at 0.2 mg and ∼0.5% at 500 mg ($T_{Rel} = T_{chl=x}/T_{chl=0}$), where x is the column-integrated concentration of chl-a. The effect on T_{Rel} for the same chl-a relative to the algae-free sea ice is approximately invariant for the different seasonal scenarios (±1.2%). The values 1–10 mg chl-a m^{-2} have additionally been modelled and are presented in the supplementary material (Fig. S1); each additional mg of chl-a appears to decrease T_{Rel} by 2–3% when columnar concentrations are ⩾10 mg chl-a m^{-2}. The effect that different thicknesses of sea ice (0.5–3.5 m) and snow (0.05–1 m) representative for the Arctic Ocean (Kurtz
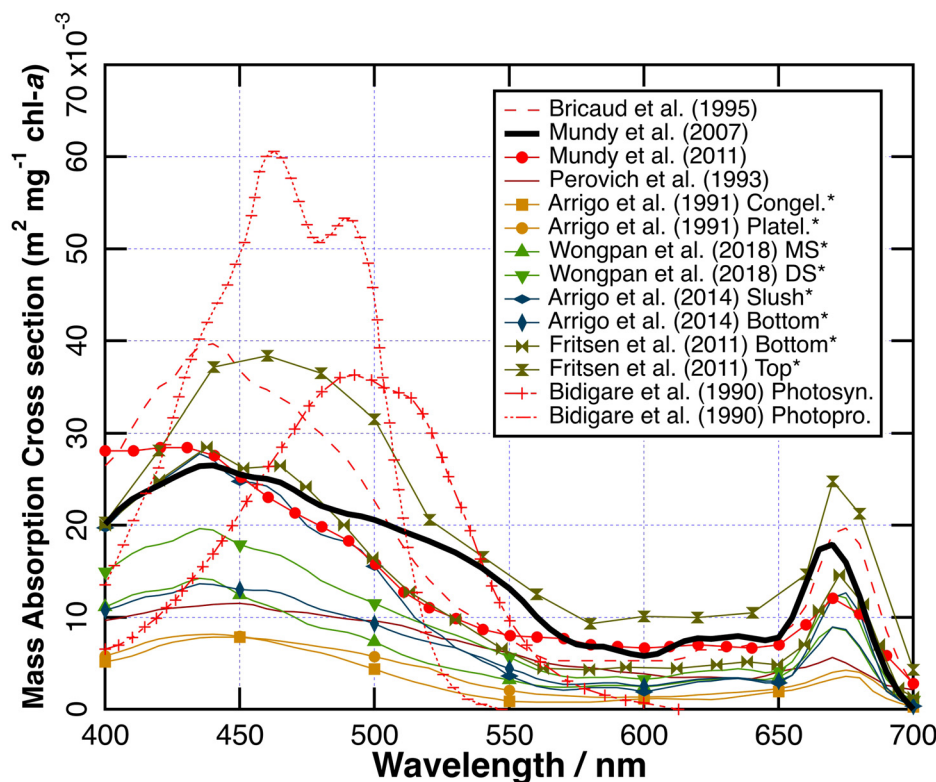

Figure 1. Ice algal chlorophyll-a biomass (Arrigo and others, 1991, 2014; Perovich, 1991; Mundy and others, 2007, 2011; Fritsen and others, 2011; Wongpan and others, 2018), phytoplankton chlorophyll-a biomass (Bricaud and others, 1995) and phytoplankton photoprotectant and photosynthetic carotenoid (Bidigare and others, 1990) mass absorption cross sections, taken from the literature. The spectral absorption cross section from Mundy and others (2007) (thick black line) has been utilised in this study. Congel. = congelation ice, Platel. = platelet ice, MS = McMurdo Sound, Antarctica, DS = Davis Station, Antarctica, Slush = surface slush, Top = top of the ice core, Bottom = bottom of the ice core, Photop. = photoprotectant carotenoid, Photosyn. = photosynthetic carotenoid.
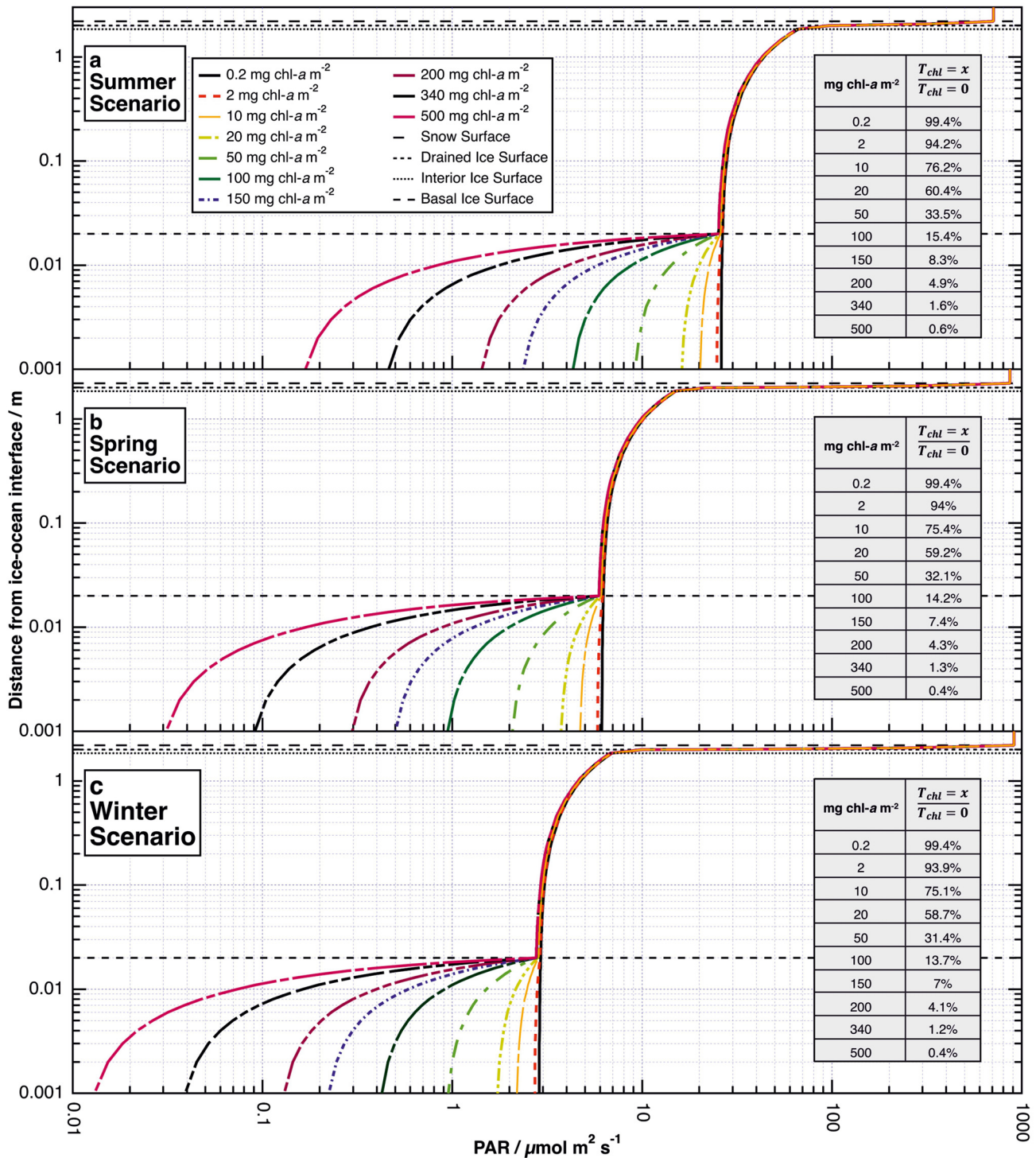
Figure 2. Modelled values of PAR through snow (0.2 m) and sea ice (2 m) layers for the summer (a), spring (b) and winter (c) scenarios. The column-integrated concentrations of sea ice algae in the basal 0.02 m of the ice increase from 0.2 to 500 mg chl-a m^{-2}. The change in T_{Rel} as column-integrated concentrations of chl-a increase relative to the algae-free sea ice ($T_{Rel} = T_{chl=x}/T_{chl=0}$) is shown for each seasonal scenario in the boxes. At the smallest column-integrated concentrations of chl-a, the effect on T_{Rel} is negligible; however, as column-integrated concentrations increase (>20 mg chl-a m^{-2}), the value of T_{Rel} is significantly reduced. The effect on T_{Rel} for the same column-integrated concentrations of chl-a is approximately invariant for the different seasonal scenarios (±1.2%).

and Harbeck, 2017) may have on T_{Rel} under typical Arctic Ocean peak basal column-integrated concentrations of chl-a (20 mg chl-a m^{-2}) (Leu and others, 2015; Lange and others, 2015) are also considered in Figure 3; all data discussed in this manuscript are available in the online repository. The change in sea ice and snow thickness causes a minor variance in T_{Rel}: ~57–63% and ~52–61%, respectively. Therefore, typical column-integrated concentrations of sea-ice algae (⩽500 mg chl-a m^{-2}) in the basal 0.02 m of the sea ice can significantly affect the value of T_{Rel},

with a minor variance due to changes in sea ice (±3.2%) and snow (±4.5%) thickness but general invariance (±1.2%) to seasonality. Bare ice was additionally modelled under cloudy conditions and clear sky conditions at a solar zenith angle of 60°; in general, there is a minor difference in the value of T_{Rel} ± 0.06–3.7%. The values of T_{Rel} are presented in the supplementary material (Table S1 and Fig. S2). Although it is improbable that the maximum chl-a values will occur during the winter scenario, they have been modelled for completeness, owing to the possibility
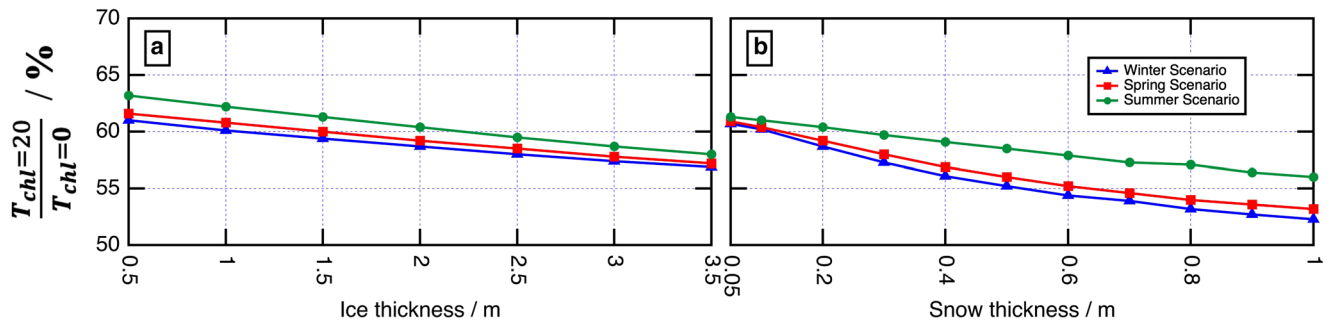
Figure 3. Changes in T_{Rel} when 20 mg chl-a m^{-2} are present at different (a) sea ice (0.5–3.5 m) and (b) snow (0.05–1 m) thickness for the winter, spring and summer scenarios. The change in sea ice and snow thickness causes a minor variance in T_{Rel}: ~57–63 and ~52–61%, respectively.

that bimodal peaks occur in March and July (Duarte and others, 2015) in the Arctic and because of the wide range in the day of year for maximum sea-ice algae chl-a concentrations (Leu and others, 2015). Similarly, the maximum considered column-integrated concentrations (340 and 500 mg chl-a m^{-2}) have only been recorded in Resolute, Canadian Arctic, and in the Antarctic, respectively, whereas all other column-integrated concentrations are more relevant for the Arctic Ocean, Greenland and Labrador Seas. However, the fundamental aim of this study is to estimate the potential effects that sea-ice algae can have on PAR transmittance in sea ice, so they have been included in this study. Ultimately, the PAR available at the ice-ocean interface is dependent on the concentration of sea-ice algae in the basal layers. When the column-integrated concentration of chl-a is low (~<10 mg chl-a m^{-2}) (e.g. the central Arctic Ocean and Greenlandic fjords), the effect on T_{Rel} is small (T_{Rel} > 75%). However, as chl-a column-integrated concentrations increase (~>10 mg chl-a m^{-2}) (e.g. the 'interior' shelves of the Arctic Ocean (Williams and Carmack, 2015)), the effect on T_{Rel} becomes more significant (T_{Rel} < 75%), with the value of T_{Rel} decreasing considerably (T_{Rel} < 10%) when column-integrated

concentrations exceed 150 mg chl-a m^{-2} (e.g. the Canadian Arctic and Antarctica) (see supplementary material Fig. S3). Consequently, when column-integrated concentrations of chl-a in sea ice exceed 10 mg chl-a m^{-2}, they should be taken into account when calculating PAR transmittance at the ice-ocean interface using existing methodologies (e.g. Redmond Roche and King, 2024); the values of T_{Rel} presented in Figure 2 can be considered as empirical reduction factors for typical algal layers of typical thickness (~0.02 m), if the light transmittance through snow and sea ice and the algal concentration is known. The authors wish to stress that although the value of T_{Rel} is mostly invariant to snow and sea-ice thickness and seasonality, the value of T is not; therefore, they must be accounted for when calculating T.

3.2. Vertical variance in algal layers

The effect that an algal layer of variable thickness can have on the value of T_{Rel} for a 0.2 m thick snowpack and 2 m thick sea ice is shown in Figure 4 for the spring scenario. Note, that having the same vertically integrated (columnar) algal concentration for a small change in depth will not have a large effect
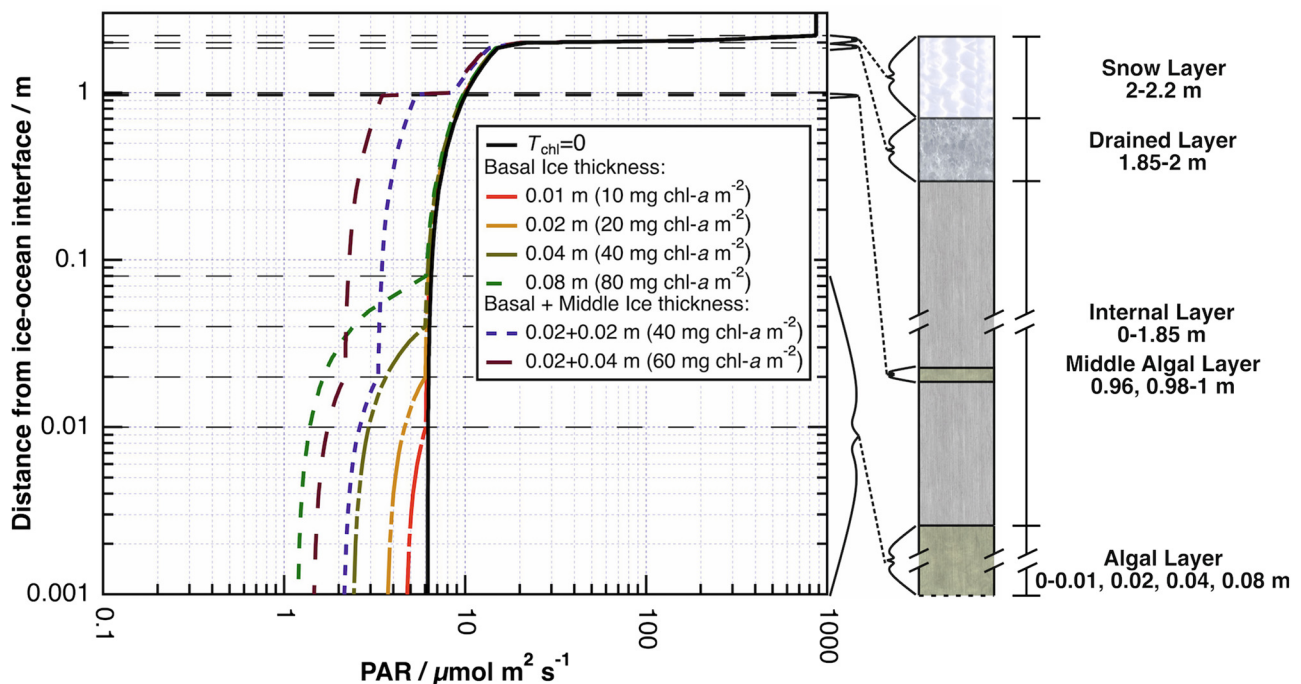

Figure 4. Modelled values of PAR transmittance through snow (0.2 m) and sea ice (2 m) layers for the spring scenario with fixed volumetric chl-a concentrations and increasing vertically integrated chl-a concentrations. The vertical extent of the basal algal thickness varies between 0.01, 0.02, 0.04 and 0.08 m; two scenarios have a 0.02 m thick basal layer and a 0.02 and 0.04 m thick middle algal layer at 0.98–1 and 0.96–1 m, respectively. A schematic of the different sea ice and snow layers is presented on the right. As the algal layer doubles in thickness, there is an approximately linear decrease in the value of PAR at the ice-ocean interface.

on the value of T. However, increasing the thickness of the algal layer and the vertically integrated chl-a concentration but maintaining the volumetric concentration will affect the value of T, which is explored in this section. Therefore, the modelled vertically integrated algae concentration varies between 10 mg chl-a m^{-2} when 0.01 m thick and 80 mg chl-a m^{-2} when 0.08 m thick, consistent with typical Arctic Ocean peak basal chl-a concentrations examined in Section 3.1 (Leu and others, 2015; Lange and others, 2015). Basal ice communities extend vertically as high as as 0.2 m (e.g. Arrigo and Sullivan, 1992; Arrigo, 2017); however, brine salinity increases and nutrient availability decreases with distance from the ice-ocean interface, whereas the 'rule of five' (i.e. brine volume $\geqslant$ 5%, ice temperature $\geqslant -5$°C, bulk salinity $\geqslant 5$) is permanently fulfilled in the basal $\sim$0.01 m (Golden and others, 1998; Leu and others, 2015). Consequently, the bottom $\sim$0.02 m of sea-ice hosts $\sim$95% of algal biomass, and higher basal ice communities will typically have an order of magnitude lower biomass (e.g. Perovich and others, 1993; Duarte and others, 2015), although there are exceptions to this (e.g. Meiners and others, 2012). Previous literature has shown that neglecting algae throughout the ice column can lead to substantial underestimations in net primary production (e.g. Duarte and others, 2015); however, aside from a study focusing on algal absorption heating sea ice (Zeebe and others, 1996), the effect on PAR transmittance remains poorly constrained. Therefore, as Figure 2 considered 0.02 m thick algal layers, the aim is to assess the sensitivity of PAR transmittance to varying algal layer thicknesses in a 1-D vertically resolved model representative of typical basal sea-ice algal communities (0.01–0.08 m), comparable to the biologically active layer used in previous studies (e.g. Tedesco and others, 2010, 2012; Tedesco and Vichi, 2014; Duarte and others, 2015; Lange and others, 2015; Leu and others, 2015; Lund-Hansen and others, 2020).

As the basal algal layer increases in thickness, the value of T decreases to 0.0054, 0.0042, 0.0028 and 0.0014 when 0.01, 0.02, 0.04 and 0.08 m thick, respectively (Fig. 4). The value of T_{Rel} decreases approximately linearly to 75.2, 59, 38.5 and 18.9% of the algae-free sea ice, respectively. While the varying thickness of the basal algae layer can affect the value of T at the base of the sea ice, it appears inconsequential on the light field near the top of the sea ice and the reflectivity of the sea ice and snow surfaces. Consequently, it may be challenging to remotely sense basal chl-a from wavelength-integrated reflectivity measurements of sea ice or snow. There can also be relatively high abundances of chl-a of varying thickness in the middle of sea-ice cores, particularly in multiyear ice where annual layers (i.e. bottom and melt pond communities) have been preserved (Lange and others, 2015) or in areas where thick snow has caused negative freeboards and surface flooding has occurred (Arrigo, 2017). While surface flooding from negative freeboards is unusual in the Arctic, it occurs in up to 30% of Antarctic sea ice (Wadhams and others, 1987; Leu and others, 2015). Thus, a 0.02 m thick basal algae layer is modelled with a 0.02 and 0.04 m thick internal algae layer at 0.98–1 and 0.96–1 m in the sea ice, respectively (Fig. 4). The presence of the middle algae layer causes the value of T_{Rel} to decrease to 62.3 and 41.8% from the top to the bottom of the 0.02 and 0.040 m layers, respectively. The decrease in the value of T_{Rel} in the mid-ice algal layers is analogous to the decrease from the top to bottom with basal algal layers of the same thickness: 60.7 and 39.7%, respectively. The value of T also appears to be largely unaffected by the vertical position of the algae layers in the ice, with the 0.04 m thick basal layer yielding a very similar value of T (0.0028) to the combined 0.02 m basal and 0.02 m middle layers combined (0.0024).

4. Conclusions

Sea-ice algae can considerably affect the transmittance of PAR, T, from the snow surface to the ice-ocean interface. The value of T will decrease as the column-integrated concentration of sea-ice algae within the ice increases: when a 0.02 m thick sea-ice algae layer is modelled in the base of the ice, the transmittance value relative to the algae-free sea ice, T_{Rel}, decreases to between 99.4% (0.2 mg chl-a m^{-2}) and 0.5% (500 mg chl-a m^{-2}). The basal concentration of algae does not affect the wavelength-integrated reflectivity of sea ice or snow above it, leading to potential challenges in remotely sensing chl-a from top of the ice or snow. The decrease in T is also dependent on the thickness of the ice algae layer. When the volumetric chl-a concentration in the ice algae layer is fixed and the layer thickness is doubled, the decrease in T_{Rel} is approximately linear: e.g. 59, 38.5 and 18.9%, at 0.02, 0.04 and 0.08 m thickness, respectively. However, the bottom $\sim$0.01 m of sea ice permanently fulfils the 'rule of five'; consequently, 95% of ice algae biomass is usually present in the basal $\sim$0.02 m. Therefore, when a typical 0.02 m thick algae layer has a low column-integrated concentration of chl-a ($\sim$<10 mg chl-a m^{-2}) (e.g. the central Arctic Ocean and Greenlandic fjords), the effect on the value of T_{Rel} is small ($T_{\text{Rel}} > 75$%). At higher column-integrated concentrations ($\sim$>10 mg chl-a m^{-2}) (e.g. the 'interior' shelves of the Arctic Ocean, the Canadian Arctic and Antarctica), the effect can be significant ($T_{\text{Rel}} < 75$%), and chl-a should be taken into account when predicting T.

References

Alexandrov V, Sandven S, Wahlin J and Johannessen OM (2010) The relation between sea ice thickness and freeboard in the Arctic. *The Cryosphere* **4**(3), 373–380. doi: 10.5194/tc-4-373-2010

Arrigo KR (2017) Sea ice as a habitat for primary producers. In Thomas DN (ed.), *Sea Ice*. Oxford, UK: Wiley Blackwell, p. 652.

Arrigo KR and Sullivan CW (1992) The influence of salinity and temperature covariation on the photophysiological characteristics of Antarctic sea ice microalgae. *Journal of Phycology* **28**, 746–756. doi: 10.1111/j.0022-3646.1992.00746.x

Arrigo KR, Sullivan CW and Kremer JN (1991) A bio-optical model of Antarctic sea ice. *Journal of Geophysical Research: Oceans* **96**(C6), 10581–10592. doi: 10.1029/91JC00455

Arrigo KR, Brown ZW and Mills MM (2014) Sea ice algal biomass and physiology in the Amundsen Sea, Antarctica. *Elementa: Science of the Anthropocene* **2**(1), 28. doi: 10.12952/journal.elementa.000028

Bidigare RR, Ondrusek ME, Morrow JH and Kiefer DA (1990) In-vivo absorption properties of algal pigments, in Ocean Optics. *Proceedings of the SPIE, Volume* 1302, pp. 290–302. doi: 10.1117/12.21451

Bricaud A, Babin M, Morel A and Claustre H (1995) Variability in the chlorophyll-specific absorption coefficients of natural phytoplankton: analysis and parameterization. *Journal of Geophysical Research: Oceans* **100**(C7), 13321–13332. doi: 10.1029/95JC00463

Cimoli E, Meiners KM, Lund-Hansen LC and Lucieer V (2017) Spatial variability in sea-ice algal biomass: an under-ice remote sensing perspective.

Advances in Polar Science **28**(4), 268–296. doi: 10.13679/j.advps.2017.4. 00268

Cota GF and Smith R (1991) Ecology of bottom ice algae: II. Dynamics, distributions and productivity. *Journal of Marine Systems* **2**(3–4), 279–295. doi: 10.1016/0924-7963(91)90037-U

Cota GF, Legendre L, Gosselin M and Ingram RG (1991) Ecology of bottom ice algae: I. Environmental controls and variability. *Journal of Marine Systems* **2**, 257–277. doi: 10.1016/0924-7963(91)90036-T

Doherty SJ, Warren SG, Grenfell TC, Clarke AD and Brandt RE (2010) Light absorbing impurities in Arctic snow. *Atmospheric Chemistry and Physics* **10**(23), 11647–11680. doi: 10.5194/acp-10-11647-2010

Duarte P and 5 others (2015) The importance of vertical resolution in sea ice algae production models. *Journal of Marine Systems* **145**, 69–90. doi: 10.1016/j.jmarsys.2014.12.004

Ehn JK and Mundy CJ (2013) Assessment of light absorption within highly scattering bottom sea ice from under-ice light measurements: implications for Arctic ice algae primary production. *Limnology & Oceanography* **58**(3), 893–902. doi: 10.4319/lo.2013.58.3.0893

Flanner MG and 9 others (2021) SNICAR-ADv3: a community tool for modeling spectral snow albedo. *Geoscientific Model Development* **14**, 7673–7704. doi: 10.5194/gmd-14-7673-2021

France JL, King MD and MacArthur A (2010) A photohabitable zone in the Martian snowpack? A laboratory and radiative-transfer study of dusty water–ice snow. *Icarus* **207**(1), 133–139. doi: 10.1016/j.icarus.2009.11.026

France JL and 7 others (2011) Snow optical properties at Dome C (Concordia), Antarctica; implications for snow emissions and snow chemistry of reactive nitrogen. *Atmospheric Chemistry and Physics* **11**, 9787–9801. doi: 10.5194/acp-11-9787-2011

Fritsen CH, Iturriaga R and Sullivan CW (1992) Influence of particulate matter on spectral irradiance fields and energy transfer in the eastern Arctic Ocean, in Ocean Optics 11. *Proceedings of the SPIE, Volume* 1750, pp. 527–541. doi: 10.1117/12.140679

Fritsen CH, Wirthlin ED, Momberg DK, Lewis MJ and Ackley SF (2011) Bio-optical properties of Antarctic pack ice in the early austral spring. *Deep Sea Research Part II: Topical Studies in Oceanography* **58**, 1052–1061. doi: 10.1016/j.dsr2.2010.10.028

Golden KM, Ackley SF and Lytle VI (1998) The percolation phase transition in sea ice. *Science* **282**, 2238–2241. doi: 10.1126/science.282.5397.2238

Gradinger RR, Kaufman MR and Bluhm BA (2009) Pivotal role of sea ice sediments in the seasonal development of near-shore Arctic fast ice biota. *Marine Ecology Progress Series* **394**, 49–63. doi: 10.3354/meps08320

Grenfell TC and Maykut GA (1977) The optical properties of ice and snow in the Arctic Basin. *Journal of Glaciology* **18**, 445–463. doi: 10.3189/S0022143000021122

Grenfell TC, Light B and Sturm M (2002) Spatial distribution and radiative effects of soot in the snow and sea ice during the SHEBA experiment. *Journal of Geophysical Research: Oceans* **107**, SHE 7-1–SHE 7-7. doi: 10.1029/2000JC000414

Hancke K and 6 others (2018) Extreme low light requirement for algae growth underneath sea ice: a case study from Station Nord, NE Greenland. *Journal of Geophysical Research: Oceans* **123**, 985–1000. doi: 10.1002/2017JC013263

Hand K, Chyba C, Priscu J, Carlson R and Nealson K (2009) Astrobiology and the potential for life on Europa. In Pappalardo RT, McKinnon WB and Khurana K (eds), *Europa*. Tucson, USA: University of Arizona Press, pp. 589–629.

Hill V, Light B, Steele M and Sybrandy AL (2022) Contrasting sea-ice algae blooms in a changing Arctic documented by autonomous drifting buoys. *Journal of Geophysical Research: Oceans* **127**, e2021JC017848. doi: 10.1029/2021JC017848

Jiao C and 28 others (2014) An Aero-Com assessment of black carbon in Arctic snow and sea ice. *Atmospheric Chemistry and Physics* **14**, 2399–2417. doi: 10.5194/acp-14-2399-2014

Katlein C, Nicolaus M and Petrich C (2014) The anisotropic scattering coefficient of sea ice. *Journal of Geophysical Research: Oceans* **119**, 842–855. doi: 10.1002/2013JC009502

King MD, France J, Fisher F and Beine H (2005) Measurement and modelling of UV radiation penetration and photolysis rates of nitrate and hydrogen peroxide in Antarctic sea ice: an estimate of the production rate of hydroxyl radicals in first-year sea ice. *Journal of Photochemistry and Photobiology A: Chemistry* **176**, 39–49. doi: 10.1016/j.jphotochem.2005.08.032

Kurtz N and Harbeck J (2017) CryoSat-2 Level-4 Sea Ice Elevation, Freeboard, and Thickness, Version 1 [Data Set]. Boulder, CO, USA:

NASA National Snow and Ice Data Center Distributed Active Archive Center. doi: 10.5067/96JO0KIFDAS8

Lamare ML, Lee-Taylor J and King MD (2016) The impact of atmospheric mineral aerosol deposition on the albedo of snow & sea ice: are snow and sea ice optical properties more important than mineral aerosol optical properties? *Atmospheric Chemistry and Physics* **16**, 843–860. doi: 10.5194/acp-16-843-2016

Lamare ML, Hedley JD and King MD (2023) The effects of surface roughness on the calculated, spectral, conical-conical reflectance factor as an alternative to the bidirectional reflectance distribution function of bare sea ice. *The Cryosphere* **17**(2), 737–751. doi: 10.5194/tc-17-737-2023

Lange BA and 8 others (2015) Comparing springtime ice-algal chlorophyll a and physical properties of multi-year and first-year sea ice from the Lincoln Sea. *PLoS ONE* **10**(4), e0122418. doi: 10.1371/journal.pone.0122418

Lavoie D, Denman K and Michel C (2005) Modeling ice-algal growth and decline in a seasonally ice-covered region of the Arctic (Resolute Passage, Canadian Archipelago). *Journal of Geophysical Research: Oceans* **110**, C11009. doi: 10.1029/2005JC002922

Lee-Taylor J and Madronich S (2002) Calculation of actinic fluxes with a coupled atmosphere–snow radiative transfer model. *Journal of Geophysical Research: Atmospheres* **107**, ACH 22-1–ACH22-10. doi: 10.1029/2002JD002084

Leu E and 7 others (2015) Arctic spring awakening – steering principles behind the phenology of vernal ice algal blooms. *Progress in Oceanography* **139**, 151–170. doi: 10.1016/j.pocean.2015.07.012

Light B, Eicken H, Maykut GA and Grenfell TC (1998) The effect of included particulates on the spectral albedo of sea ice. *Journal of Geophysical Research: Oceans* **103**, 27739–27752. doi: 10.1029/98JC02587

Light B, Grenfell TC and Perovich DK (2008) Transmission and absorption of solar radiation by Arctic sea ice during the melt season. *Journal of Geophysical Research: Oceans* **113**, C03023. doi: 10.1029/2006jc003977

Light B, Perovich DK, Webster MA, Polashenski C and Dadic R (2015) Optical properties of melting first-year Arctic sea ice. *Journal of Geophysical Research: Oceans* **120**, 7657–7675. doi: 10.1002/2015JC011163

Light B and 10 others (2022) Arctic sea ice albedo: spectral composition, spatial heterogeneity, and temporal evolution observed during the MOSAiC drift. *Elementa: Science of the Anthropocene* **10**(1), 000103. doi: 10.1525/elementa.2021.000103

Lim SM, Payne CM, van Dijken GL and Arrigo KR (2022) Increases in Arctic sea ice algal habitat, 1985–2018. *Elementa Science of the Anthropocene* **10**(1), 00008. doi: 10.1525/elementa.2022.00008

Lund-Hansen LC, Søgaard DH, Sorrell BK, Gradinger R and Meiners KM (2020) *Arctic Sea Ice Ecology: Seasonal Dynamics in Algal and Bacterial Productivity*. Cham, Switzerland: (eds) Springer Polar Sciences.

Lund-Hansen LC, Bjerg-Nielsen M, Stratmann T, Hawes I and Sorrell BK (2021) Upwelling irradiance below sea ice – PAR intensities and spectral distributions. *Journal of Marine Science and Engineering* **9**, 830. doi: 10.3390/jmse9080830

Madronich S and Flocke S (1998) The role of solar radiation in atmospheric chemistry. In Boule P (ed.), *Handbook of Environmental Chemistry*. New York, USA: Springer-Verlag, pp. 1–26.

Marks AA and King MD (2013) The effects of additional black carbon on the albedo of Arctic sea ice: variation with sea ice type and snow cover. *The Cryosphere* **7**, 1193–1204. doi: 10.5194/tc-7-1193-2013

Marks AA and King MD (2014) The effect of snow/sea ice type on the response of albedo and light penetration depth (e-folding depth) to increasing black carbon. *The Cryosphere* **8**, 1625–1638. doi: 10.5194/tc-8-1625-2014

Marks AA, Lamare ML and King MD (2017) Optical properties of sea ice doped with black carbon – an experimental and radiative-transfer modelling comparison. *The Cryosphere* **11**, 2867–2881. doi: 10.5194/tc-11-2867-2017

Meiners KM (2012) Chlorophyll a in Antarctic sea ice from historical ice core data. *Geophysical Research Letters* **39**(21), L21602. doi: 10.1029/2012GL053478

Melnikov IA, Kolosova EG, Welch HE and Zhitina LS (2002) Sea ice biological communities and nutrient dynamics in the Canada Basin of the Arctic Ocean. *Deep Sea Research Part I: Oceanographic Research Papers* **49**, 1623–1649. doi: 10.1016/S0967-0637(02)00042-0

Mobley C and 5 others (1998) Modeling light propagation in sea ice. *IEEE Transactions on Geoscience and Remote Sensing* **36**(5), 1743–1749, 1998. doi: 10.1109/36.718642

Morel A and Bricaud A (1981) Theoretical results concerning light absorption in a discrete medium, and application to specific absorption of phytoplankton. *Deep Sea Research Part A. Oceanographic Research Papers* **28**(11), 1375–1393. doi: 10.1016/0198-0149(81)90039-X

Mundy CJ, Ehn JK, Barber DG and Michel C (2007) Influence of snow cover and algae on the spectral dependence of transmitted irradiance through Arctic landfast first-year sea ice. *Journal of Geophysical Research: Oceans* **112**, C03007. doi: 10.1029/2006JC003683

Mundy CJ and 11 others (2011) Characteristics of two distinct high-light acclimated algal communities during advanced stages of sea ice melt. *Polar Biology* **34**, 1869–1886. doi: 10.1007/s00300-011-0998-x

Perovich DK (1990) Theoretical estimates of light reflection and transmission by spatially complex and temporally varying sea ice covers. *Journal of Geophysical Research: Oceans* **95**, 9557–9567. doi: 10.1029/JC095iC06p09557

Perovich DK (1991) Seasonal changes in sea ice optical properties during fall freeze-up. *Cold Regions Science and Technology* **19**, 261–273. doi: 10.1016/0165-232X(91)90041-E

Perovich DK (1996) *The Optical Properties of Sea Ice, Monogr 96–1.* Hanover, NH, USA: U. S. Cold Regions Research and Engineering Lab, p. 25.

Perovich DK, Cota GF, Maykut GA and Grenfell TC (1993) Bio-optical observation of first-year Arctic sea ice. *Geophysical Research Letters* **20**(11), 1059–1062. doi: 10.1029/93GL01316

Perovich DK, Roesler CS and Pegau WS (1998) Variability in Arctic sea ice optical properties. *Journal of Geophysical Research: Oceans* **103**, 1193–1208. doi: 10.1029/97JC01614

Petrich C, Nicolaus M and Gradinger R (2012) Sensitivity of the light field under sea ice to spatially inhomogeneous optical properties and incident light assessed with three-dimensional Monte Carlo radiative transfer simulations. *Cold Regions Science and Technology* **73**, 1–11. doi: 10.1016/j.coldregions.2011.12.004

Popova EE and 6 others (2010) Control of primary production in the Arctic by nutrients and light: insights from a high resolution ocean general circulation model. *Biogeosciences Discussions* **7**, 5557–5620. doi: 10.5194/bgd-7-5557-2010

Redmond Roche BH and King MD (2022) Quantifying the effects of background concentrations of crude oil pollution on sea ice albedo. *The Cryosphere* **16**, 3949–3970. doi: 10.5194/tc-16-3949-2022

Redmond Roche BH and King MD (2024) Calculations of Arctic ice-ocean interface photosynthetically active radiation (PAR) transmittance. *Earth and Space Science* **11**, e2023EA002948. doi: 10.1029/2023EA002948

Réveillet M and 11 others (2022) Black carbon and dust alter the response of mountain snow cover under climate change. *Nature Communications* **13**, 5279. doi: 10.1038/s41467-022-32501-y

Reynolds RT, Squyres SW, Colburn DS and McKay C (1983) On the habitability of Europa. *Icarus* **56**, 246–254. doi: 10.1016/0019-1035(83)90037-4

Riaux-Gobin C, Treguer P, Poulin M and Vetion G (2000) Nutrients, algal biomass and communities in land-fast ice and seawater off Adelie Land (Antarctica). *Antarctic Science* **12**, 160–171. doi: 10.1017/S0954102000000213

Søgaard DH and 5 others (2010) Autotrophic and heterotrophic activity in Arctic first-year sea ice: seasonal study from Malene Bight, SW Greenland. *Marine Ecology Progress Series* **419**, 31–45. doi: 10.3354/meps08845

Søgaard DH, Deming JW, Meire L and Rysgaard S (2019) Effects of microbial processes and $CaCO_3$ dynamics on inorganic carbon cycling in snow-covered Arctic winter sea ice. *Marine Ecology Progress Series* **611**, 31–44. doi: 10.3354/meps12868

SooHoo JB and 5 others (1987) Spectral light absorption and quantum yield of photosynthesis in sea ice microalgae and a bloom of *Phaeocystis pouchetii* from McMurdo Sound, Antarctica. *Marine Ecology Progress Series* **39**(2), 175–189.

Stamnes K, Tsay S-C, Wiscombe W and Jayaweera K (1988) Numerically stable algorithm for discrete-ordinate-method radiative transfer in multiple scattering and emitting layered media. *Applied Optics* **27**, 2502–2509. doi: 10.1364/AO.27.002502

Stroeve J and 9 others (2021) A multi-sensor and modeling approach for mapping light under sea ice during the ice-growth season. *Frontiers in Marine Science* **7**, 592337. doi: 10.3389/fmars.2020.592337

Tedesco L and Vichi M (2014) Sea ice biogeochemistry: a guide for modellers. *PLoS ONE* **9**(2), e89217. doi: 10.1371/journal.pone.0089217

Tedesco L, Vichi M, Haapala J and Stipa T (2010) A dynamic biologically active layer for numerical studies of the sea ice ecosystem. *Ocean Modelling* **35**, 89–104. doi: 10.1016/j.ocemod.2010.06.008

Tedesco L, Vichi M and Thomas DN (2012) Process studies on the ecological coupling between sea ice algae and phytoplankton. *Ecological Modelling* **226**, 120–138. doi: 10.1016/j.ecolmodel.2011.11.011

Trodahl HJ, Buckley RG and Brown S (1987) Diffusive transport of light in sea ice. *Applied Optics* **26**(15), 3005–3011. doi: 10.1364/AO.26.003005

Vérin G, Domine F, Babin M, Picard G and Arnaud L (2022) Metamorphism of snow on Arctic sea ice during the melt season: impact on spectral albedo and radiative fluxes through snow. *The Cryosphere* **16**, 3431–3449. doi: 10.5194/tc-16-3431-2022

Wadhams P, Lange MA and Ackley SF (1987) The ice thickness distribution across the Atlantic sector of the Antarctic Ocean in midwinter. *Journal of Geophysical Research: Oceans* **92**(C13), 14535–14552. doi: 10.1029/JC092iC13p14535

Wang L, Jiang L, Xing X, Chen Y and Meng Q (2020) The effects of pheophytin a on absorption properties of phytoplankton in Dalian Bay, China. *IOP Conference Series: Earth and Environmental Science* **428**, 012048. doi: 10.1088/1755-1315/428/1/012048

Warren SG (1982) Optical properties of snow. *Reviews of Geophysics and Space Physics* **20**, 67–89. doi: 10.1029/RG020i001p00067

Warren SG (2019) Optical properties of ice and snow. *Physical Transactions of the Royal Society A* **377**, 20180161. doi: 10.1098/rsta.2018.0161

Warren SG and Brandt RE (2008) Optical constants of ice from the ultraviolet to the microwave: a revised compilation. *Journal of Geophysical Research: Atmospheres* **113**, D14220. doi: 10.1029/2007JD009744

Weckström K and 7 others (2020) Improving the paleoceanographic proxy tool kit – on the biogeography and ecology of the sea ice-associated species *Fragilariopsis oceanica, Fragilariopsis reginae-jahniae* and *Fossula arctica* in the northern North Atlantic. *Marine Micropaleontology* **157**, 101860. doi: 10.1016/j.marmicro.2020.101860

Welch HE and Bergmann MA (1989) Seasonal development of ice algae and its prediction from environmental factors near Resolute, N.W.T., Canada. *Canadian Journal of Fisheries and Aquatic Science* **46**(10), 1793–1804. doi: 10.1139/f89-227

Williams WJ and Carmack EC (2015) The 'interior' shelves of the Arctic Ocean: physical oceanographic setting, climatology and effects of sea-ice retreat on cross-shelf exchange. *Progress in Oceanography* **139**, 24–41. doi: 10.1016/j.pocean.2015.07.008

Wongpan P and 8 others (2018) Estimation of Antarctic land-fast sea ice algal biomass and snow thickness from under-ice radiance spectra in two contrasting areas. *Journal of Geophysical Research: Oceans* **123**, 1907–1923. doi: 10.1002/2017JC013711

Zeebe R and 5 others (1996) Modeling the heating and melting of sea ice through light absorption by microalgae. *Journal of Geophysical Research* **101**(C1), 1163–1181. doi: 10.1029/95JC02687

Zhang Q and 6 others (2020) Freeboard height and snow depth observed by floating GPS on land-fast sea ice in Nella Fjord, Antarctica. *Annals of Glaciology* **61**(82), 227–239. doi: 10.1017/aog.2020.41